Electronic Supporting Information for

Design of Superhalogens Using Core-Shells Structure Model

Zhifeng Liu[1,2], Xiaojuan Liu[1], Jijun Zhao[2,3*]

[1] School of Physical Science and Technology, Inner Mongolia University, Hohhot 010021, China

[2] Beijing Computational Science Research Center, Beijing 100094, China

[3] Key Laboratory of Materials Modification by Laser, Ion and Electron Beams (Dalian University of Technology), Ministry of Education, Dalian 116024, China

* Address correspondence to Prof. Jijun Zhao: zhaojj@dlut.edu.cn

CONTENT:

S1. The sphere-like polyhedral geometries of B_nN_n cage clusters

The structural components (polyhedron rings) of B_nN_n (e.g., n=12, 16, 24, 28, 36) cage clusters are:

$B_{12}N_{12}$: 6×4MR+8×6MR,

$B_{16}N_{16}$: 6×4MR+12×6MR,

$B_{24}N_{24}$: 12×4MR+8×6MR+6×8MR,

$B_{28}N_{28}$: 6×4MR+24×6MR,

$B_{36}N_{36}$: 6×4MR+32×6MR,

where the number of 4MR (N_{4MR}), 6MR (N_{6MR}) and 8MR (N_{8MR}) obeys the equations of $N_{6MR}= n - 4 - 2N_{8MR}$ and $N_{4MR}= 6 + N_{8MR}$.[1]

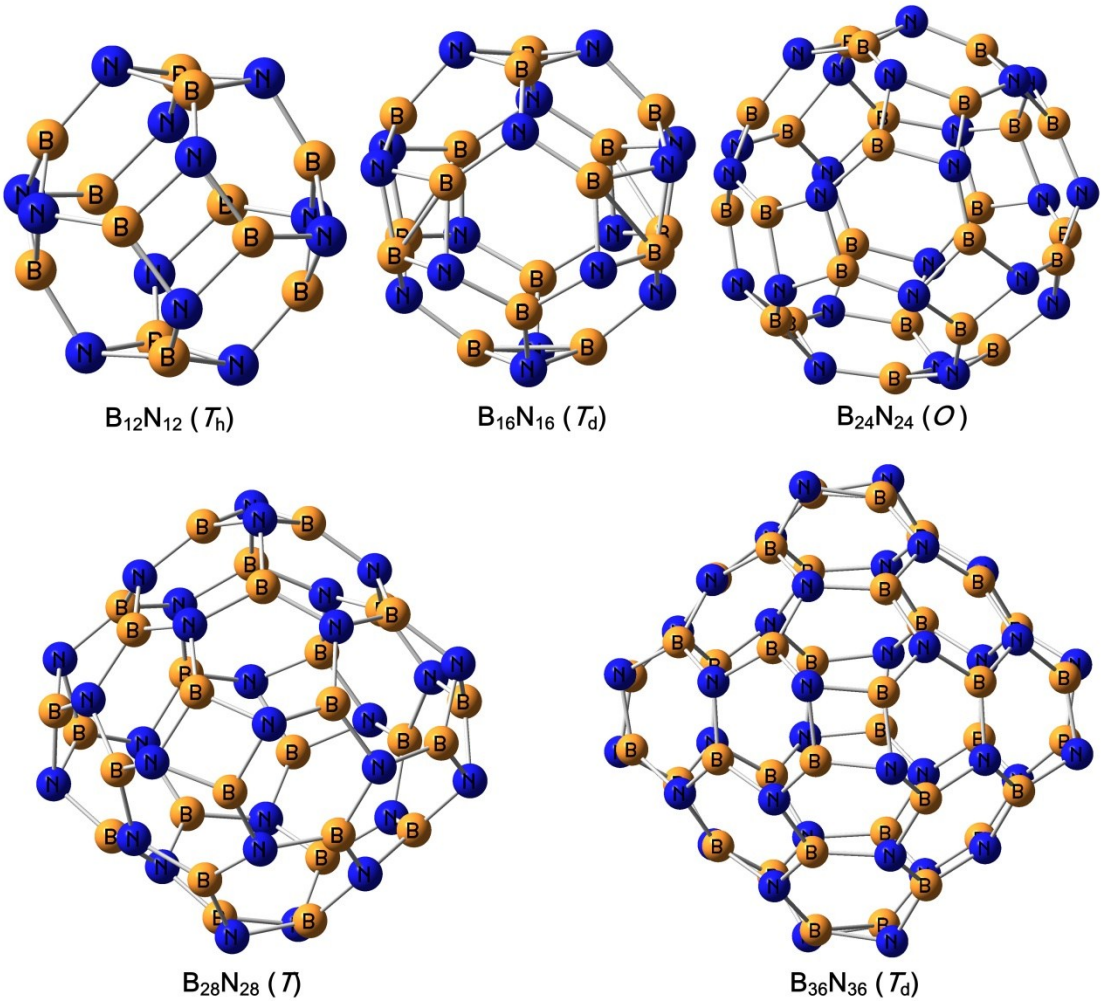

Fig. S1 The sphere-like polyhedral structures with high symmetry for B_nN_n (n=12, 16, 24, 28, 36) clusters. The symmetries are presented in the corresponding parenthesis.

S2. Superhalogen properties of the endohedral cage clusters $X@Y_{12}Z_{12}$

As listed in Table S1, all the VDEs are much larger than that of Cl^- (3.72 eV by B3LYP/6-311+G(d) in this work, 3.61 eV in previous experiment[2]). Also the EA of the corresponding neutral cluster is larger than that of Cl atom (3.72 eV in this work). Thus, all these endohedral $X@Y_{12}Z_{12}$ clusters are superhalogen. This is a powerful proof for our assumption that new superhalogens can be constructed from the II-VI and III-V cage-like cluster by using the proposed core-shells structure model. Moreover, the differences between EA and VDE of all the considered $X@Y_{12}Z_{12}$ clusters are small, ranging from 0.11 eV to 0.31 eV. That is to say, the structural relaxations caused by change of charging state are insignificant.

Table S1 EAs, VDEs of the corresponding anionic cluster, fragmentation energies (ΔE), binding energies per atom (E_b), and HOMO-LUMO gaps (E_g) for the endohedrally doped $X@Y_{12}Z_{12}$ (X=F, Cl, Br, YZ=AlN, GaN, ZnS, ZnO) clusters.

Clusters	EAs (eV)	VDEs (eV)	ΔE (eV)	E_b (eV)	E_g (eV)
$F@Al_{12}N_{12}$	4.26	4.55	–6.44	–4.23	3.88
$Cl@Al_{12}N_{12}$	4.25	4.48	–2.47	–4.08	3.70
$Br@Al_{12}N_{12}$	3.99	4.26	–0.69	–4.01	3.54
$F@Ga_{12}N_{12}$	4.41	4.71	–6.92	–3.21	2.90
$Cl@Ga_{12}N_{12}$	4.38	4.67	–3.53	–3.08	2.67
$Br@Ga_{12}N_{12}$	4.21	4.52	–1.88	–3.01	2.56
$F@Zn_{12}S_{12}$	5.15	5.44	–7.55	–2.39	4.63
$Cl@Zn_{12}S_{12}$	5.39	5.51	–5.98	–2.34	4.59
$Br@Zn_{12}S_{12}$	5.41	5.52	–5.36	–2.31	4.52
$F@Zn_{12}O_{12}$	5.23	5.41	–6.23	–2.78	4.10
$Cl@Zn_{12}O_{12}$	5.05	5.34	–5.84	–2.71	4.07
$Br@Zn_{12}O_{12}$	4.83	5.98	–4.82	–2.67	4.04

S3. Structural parameters for the $X@B_{12}N_{12}^{q}$ (X=F, Cl, Br, q=0, −1) clusters

All the $X@B_{12}N_{12}^{q}$ (X=F, Cl, Br, q=0, −1) clusters have very similar endohedral cage-like geometries, as shown in Fig. 2d. From the structural parameters (L_{4MR} $L_{4MR\text{-}4MR}$, $D_{N\text{-}c}$ and $D_{B\text{-}c}$ in Table S2), one can see that the cage cavity is slightly expanded with respect to the pristine $B_{12}N_{12}$. For a given cluster, the corresponding $D_{N\text{-}c}$ is larger than $D_{B\text{-}c}$, indicating that it has double atomic shells. Since all the values of $D_{x\text{-}c}$ are zero, the endohedral X atom should be located at the center of the cage structure for all the endohedral clusters.

Table S2 The point group symmetry, average lengths of B-N bonds in the 4MRs (L_{4MR}, in Å), average lengths of B-N bonds linked the adjacent 4MRs ($L_{4MR\text{-}4MR}$, in Å), average distances between the N/B/X atom and the geometrical center of the cage-like cluster ($D_{N\text{-}c}$/$D_{B\text{-}c}$/$D_{X\text{-}c}$, in Å) for the endohedrally doped $X@B_{12}N_{12}^{q}$ (X=F, Cl, Br, q=0, −1) clusters. The relevant data of $B_{12}N_{12}$ are also included for comparison.

Clusters	Symmetry	L_{4MR}	$L_{4MR\text{-}4MR}$	$D_{N\text{-}c}$	$D_{B\text{-}c}$	$D_{X\text{-}c}$
$B_{12}N_{12}$	T_h	1.486	1.438	2.400	2.209	—
$F@B_{12}N_{12}$	C_i	1.498	1.459	2.448	2.205	0.000
$Cl@B_{12}N_{12}$	C_i	1.526	1.490	2.497	2.262	0.000
$Br@B_{12}N_{12}$	C_i	1.542	1.510	2.533	2.284	0.000
$F@B_{12}N_{12}^{-}$	T_h	1.502	1.460	2.444	2.188	0.000
$Cl@B_{12}N_{12}^{-}$	T_h	1.534	1.500	2.503	2.239	0.000
$Br@B_{12}N_{12}^{-}$	Ci	1.551	1.522	2.535	2.263	0.000

S4. Stability of $X@B_{12}N_{12}^{q}$ (X=F, Cl, Br, q=0, −1) clusters

For any potential applications of superhalogens, it is important to examine their various stabilities, including dynamic stability, energetic stability and thermal stability at finite temperature. The calculation of harmonic vibrational frequency shows that there are no imaginary frequencies in all of the endohedral $X@B_{12}N_{12}^{q}$ (X=F, Cl, Br, q=0, −1) clusters, implying that they are dynamically stable and belong to minima in the corresponding potential energy surface. As for energetic stability, we calculate two important physical quantities, i.e., the fragmentation energy ΔE and the average binding energy E_b:

$$\Delta E = E(X@B_{12}N_{12}) - E(X^{-}) - E(B_{12}N_{12}^{+})$$

$$E_b = \frac{E(X@B_{12}N_{12}) - E(X) - 12E(B) - 12E(N)}{25}$$

Among the considered systems, $F@B_{12}N_{12}$ holds a negative ΔE and the smallest E_b, which indicates that it is energetically stable with respect to the corresponding fragmentations. However, compared with F atom the Cl and Br atoms have larger atomic radius which may be incommensurate to the cavity size of the $B_{12}N_{12}$ cluster, thus the corresponding $Cl@B_{12}N_{12}$ and $Br@B_{12}N_{12}$ clusters have positive ΔE and lower E_b and then show energetic instability. Based on this fact, hereafter we just focus on the thermal stability of anionic $F@B_{12}N_{12}$ cluster.

The *ab initio* molecular dynamics (AIMD) simulations at 500 K were performed by using projector augmented wave (PAW) method [3] and Perdew-Burke-Ernzerhof (PBE)[4] exchange-correlation functional as implemented in the VASP code.[5] During the simulations, an energy cutoff of 500 eV was used for the plane-wave basis set. To avoid image interactions from the periodic boundary condition, a large vacuum region of 25 Å was applied to all three directions. Thus the corresponding first Brillouin zone was sampled using the Monkhorst-Pack scheme with only Γ-point. Fig. S2a presents the fluctuations of potential energies as a function of the simulation time. During the whole process of 10 ps simulations with a chosen time step of 1 fs, no structural distortion or reconstruction can be found, and the measured potential energies

oscillate around almost the same value, confirming that the structure of $F@B_{12}N_{12}^-$ is stable enough to withstand thermal turbulence up to at least 500 K.

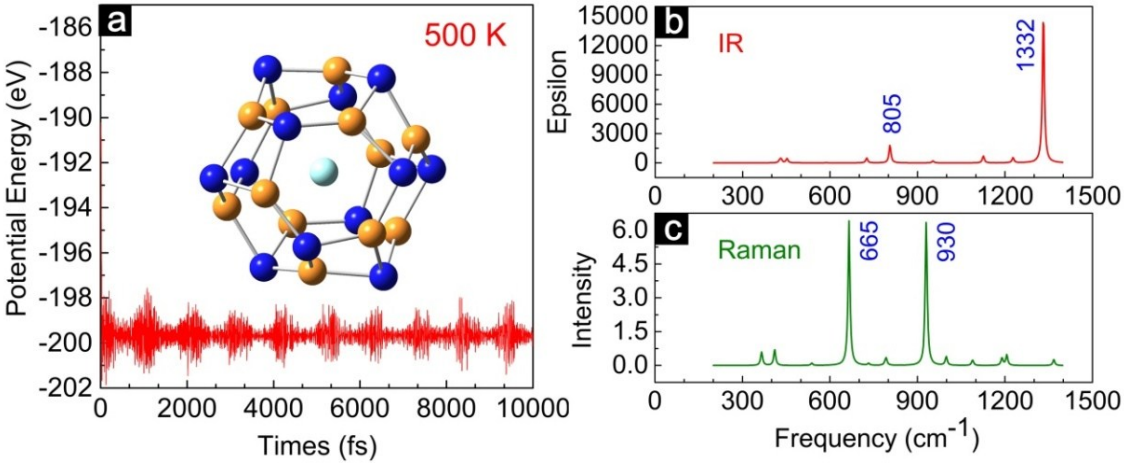

Fig. S2 Thermal stability characterized by AIMD simulation (a), and the theoretical IR (b) and Raman (c) spectra for the anionic $F@B_{12}N_{12}^-$ cluster.

To provide useful signatures for future experimental detections of anionic $F@B_{12}N_{12}$ cluster, we have simulated the infrared and Raman spectra, as is illustrated in Fig. S2b and S2c. The IR spectrum reveals two conspicuous peaks at the vibrational frequencies of 805 cm^{-1} and 1332 cm^{-1}. In the Raman spectroscopy, two prominent peaks can be found at 665 cm^{-1} and 930 cm^{-1}.

S5. Geometries and structural parameters of the Li(F@$B_{12}N_{12}$) isomers

From Fig. S3 and Table S3, one can find that the anionic components of the two Li(F@$B_{12}N_{12}$) isomers hold almost the same geometry of the individual anionic F@$B_{12}N_{12}$ (Fig. 2d).

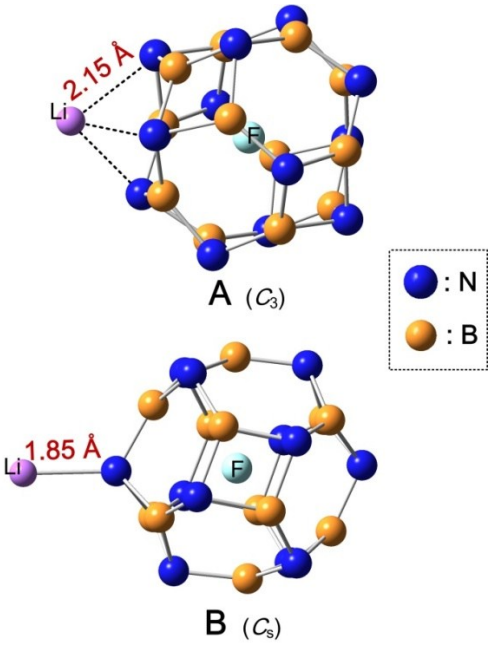

Fig. S3 Optimized geometries of the two energy low-lying Li(F@$B_{12}N_{12}$) isomers. The symmetries are presented in the parenthesis.

Table S3 The point group symmetry, the relative energy with respect to the most stable structure (E_{rel}, in eV), average lengths of B-N bonds in the 4MRs (L_{4MR}, in Å), average lengths of B-N bonds linked the adjacent 4MRs ($L_{4MR\text{-}4MR}$, in Å), average distances between the N/B/F atom and the geometrical center of the cage ($D_{N\text{-}c}$/$D_{B\text{-}c}$/$D_{F\text{-}c}$, in Å) and the shortest distance between Li atom and the superhalogen F@$B_{12}N_{12}$ ($D_{Li\text{-}SH}$, in Å) for the low-lying isomers of Li(F@$B_{12}N_{12}$) salt. The relevant data of F@$B_{12}N_{12}$ are also included for comparison.

Clusters	*Symmetry*	E_{rel}	L_{4MR}	$L_{4MR\text{-}4MR}$	$D_{N\text{-}c}$	$D_{B\text{-}c}$	$D_{F\text{-}c}$	$D_{Li\text{-}SH}$
F@$B_{12}N_{12}$	C_i		1.498	1.459	2.448	2.205	0.000	
A-Li-F@$B_{12}N_{12}$	C_3	0	1.497	1.458	2.443	2.190	0.002	2.149
B-Li-F@$B_{12}N_{12}$	C_s	0.108	1.503	1.458	2.444	2.192	0.011	1.854

S6. NBO charge distribution of the ground state of Li(F@$B_{12}N_{12}$)

By comparison (see Fig. S4 and Fig. 3b), we can find that the NBO charge distribution of anionic components of Li(F@$B_{12}N_{12}$) is very similar with that of the individual F@$B_{12}N_{12}^-$——the same B valence electron configuration ($2s^{0.46}$ $2p^{1.32}$), and very similar N valence electron configuration ($2s^{1.41}$ $2p^{4.82}$ versus $2s^{1.41}$ $2p^{4.81}$).

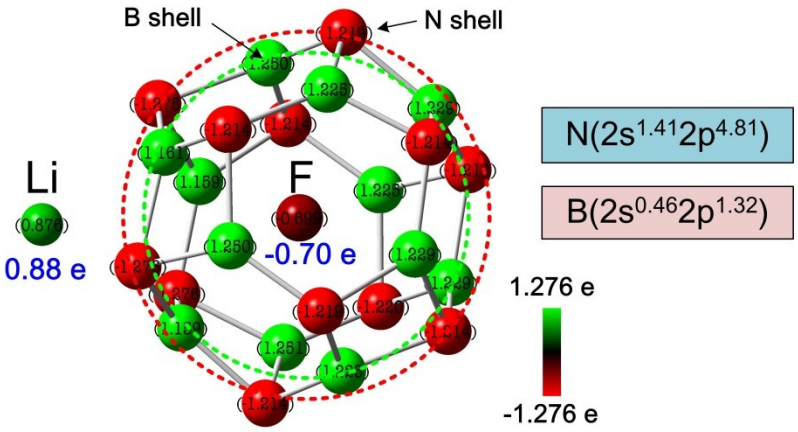

Fig. S4 The NBO charge distribution and corresponding average valence electron configurations of each B and N atom for the lowest energy structure of Li(F@$B_{12}N_{12}$) cluster. The red and green balls represent the N and B atoms, respectively; the crimson and dark green balls stand for F and Li atoms, respectively.

S7 Binding energies of Li^+ and H_2O

The detailed values corresponding to Fig. 4, calculated by B3LYP/6-311+G(d) method, are listed in Table S4. To check the sensitivity of our results to numerical method, we have repeated our calculation using the wB97XD/6-311+G(d) method (see Table S4). Except for the minor difference in value, the variational trend of relative values of different clusters at these two methods agrees with each other, giving us confidence in the conclusions.

Table S4 The calculated binding energies of Li^+ and H_2O for currently used and potential electrolytes in Li-ion batteries. For comparison, the previous results in Ref [6] at the wB97XD/6-311+G(d) level are also given.

Components	ΔE_{Li^+}		ΔE_{H2O}	
	B3LYP	wB97XD	B3LYP	wB97XD
$F@B_{12}N_{12}$	4.87	4.72	1.18	1.19
ClO_4	6.15	5.96[a]	1.035	1.02[a]
BF_4	6.23	6.08[a]	1.382	1.41[a]
PF_6	5.87	5.73[a]	1.034	1.07[a]
AsF_6	5.78	5.65[a]	1.021	1.09[a]
$FePO_4$	7.45	7.38[a]	0.918	1.04[a]
$N(SO_2F)_2$	5.93	5.82[a]	1.012	1.02[a]
$N(SO_2CF_3)_2$	6.13	6.01[a]	0.981	0.99[a]
$CB_{11}H_{12}$	5.39	5.08[a]	1.045	1.08[a]

[a] The theoretical data at wB97XD/6-311+G(d) level in Ref[6]

S8 Geometries of the H_2O-Li($F@B_{12}N_{12}$) isomers.

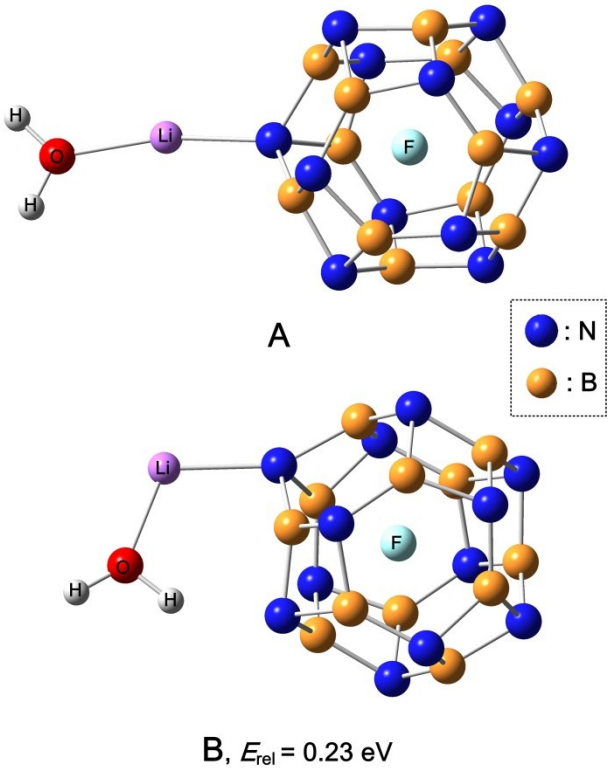

Fig. S5 Optimized low-lying energy geometries (A and B) of H_2O-Li($F@B_{12}N_{12}$) isomers. The relative energy (E_{rel}) of B with respect to the most stable structure A is 0.23 eV. No imaginary frequency has been found in the calculation of harmonic vibrational frequencies for both of them.

S9. Geometries of the Li(F@$B_{12}N_{12}$)$_2$ isomers.

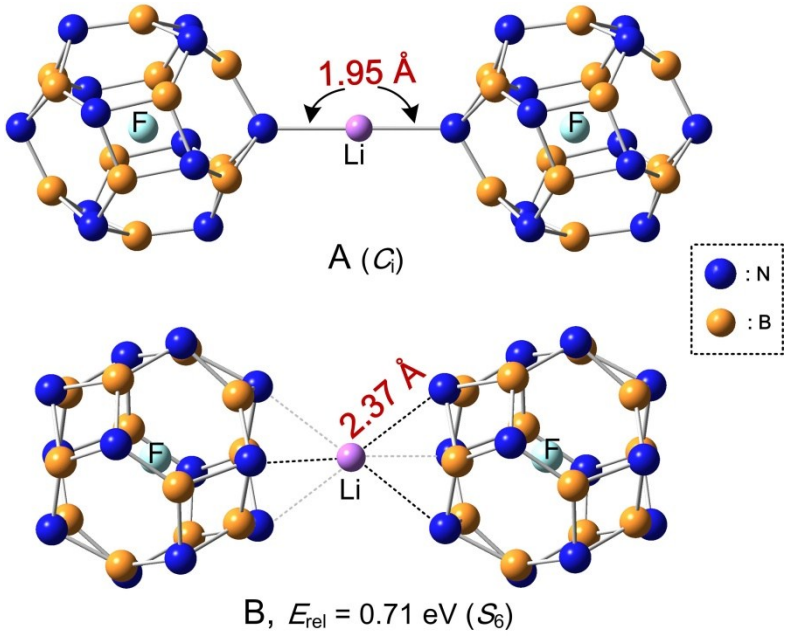

Fig. S6 Optimized low-lying energy geometries (A and B) of neutral Li(F@$B_{12}N_{12}$)$_2$ isomers. The structure of the corresponding anion is similar with that of the shown neutral one. The symmetries are presented in the parenthesis. The relative energy (E_{rel}) of B with respect to the most stable structure A is 0.71 eV. All the harmonic vibrational frequencies are positive in these two structures.

S10. NBO charge distribution and hyperhalogen properties of $Li(F@B_{12}N_{12})_2$

As discussed, the $F@B_{12}N_{12}$ needs about one extra electron to compensate the charge of outer N shell. In the ground state of $Li(F@B_{12}N_{12})_2$, the NBO charges on the metal Li atom are close to +1. Hence $Li(F@B_{12}N_{12})_2$ also needs one extra electron to compensate the charge of outer N shell in the two $F@B_{12}N_{12}$ building blocks. When an extra electron is added to the electron-deficient $Li(F@B_{12}N_{12})_2$, it will distribute over all N atoms (see Fig. S7, the unchanged electron configuration of B and changed one of N with respect to the case of neutral $Li(F@B_{12}N_{12})_2$), which have larger phase space with respect to $F@B_{12}N_{12}$. Thus, the electron-electron repulsion in $Li(F@B_{12}N_{12})_2$ will be weaker than that in $F@B_{12}N_{12}$, resulting in that $Li(F@B_{12}N_{12})_2$ holds larger VDE and displays the novel hyperhalogen properties.

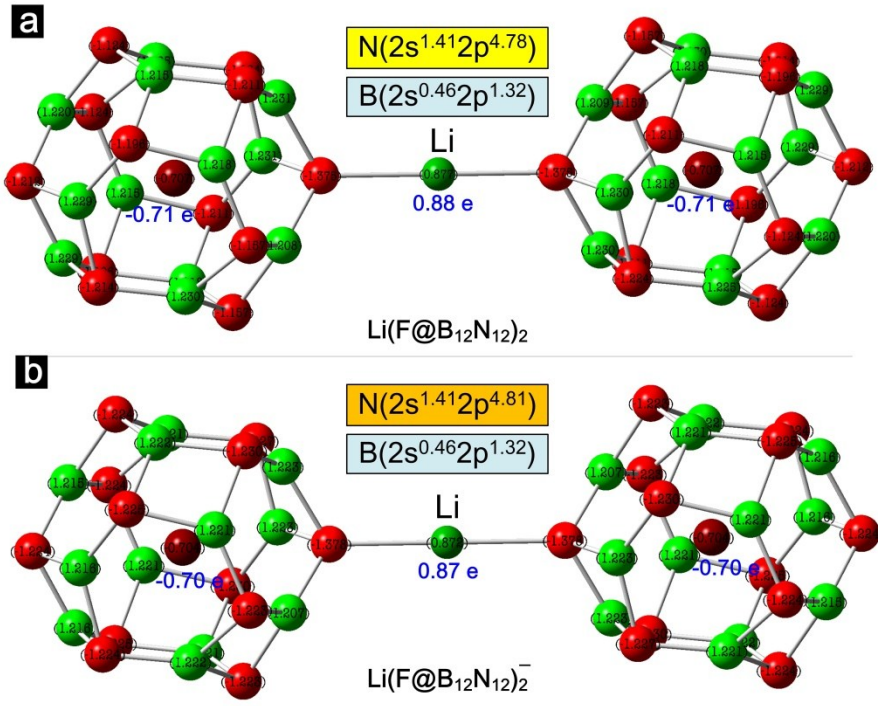

Fig. S7 The NBO charge distribution and corresponding average valence electron configurations of each B and N atom for the lowest energy structure of $Li(F@B_{12}N_{12})_2$ (a) and $Li(F@B_{12}N_{12})_2^-$ (b) clusters. The red and green balls represent the N and B atoms, respectively; the crimson ball stands for F atom.

Supplementary References

1 J. M. Matxain, L. A. Eriksson, J. M. Mercero, X. Lopez, M. Piris, J. M. Ugalde, J. Poater, E. Matito and M. Solà, *J. Phys. Chem. C*, 2007, **111**, 13354-13360.

2 X. B. Wang, C. F. Ding, L. S. Wang, A. I. Boldyrev and J. Simons, *J. Chem. Phys.*, 1999, **110**, 4763-4771.

3 P. E. Blöchl, *Phys. Rev. B*, 1994, **50**, 17953-17979.

4 J. P. Perdew, K. Burke and M. Ernzerhof, *Phys. Rev. Lett.*, 1996, **77**, 3865-3868.

5 G. Kresse and J. Furthmüller, *Phys. Rev. B*, 1996, **54**, 11169-11186.

6 S. Giri, S. Behera and P. Jena, *Angew. Chem. Int. Ed.*, 2014, **53**, 13916-13919.